VARIABLE SENSITIVITY MOIRE INTERFEROMETRY

by

Helen Johnson-Cole, James H. Bennewitz, and John A. Gilbert[1]

Abstract

This paper demonstrates that optical microlithography can be used to produce a crossed grating which diffracts light into multiple orders sufficient to record moire interferograms with sensitivities ranging from 2.0 to 0.285 μm/fringe. The grating profile produced by the method is analyzed to establish the diffraction efficiency in each diffraction order and generalized expressions are given for variable sensitivity moire interferometry. Experimental tests are conducted to verify analytical arguments. In one of these tests, two different diffraction order pairs are used simultaneously to verify that surface displacement can be measured at different sensitivities.

Introduction

In 1965, Dally and Riley[1] wrote: "If and when higher quality line arrays with line spacings of 10,000 to 30,000 lines/in. become available, the moire method may see more general usage in a wider range of experimental stress analysis." That level of technical sophistication was met when Post proposed an approach to in-plane surface displacement measurement called moire interferometry.[2] The method involves the transfer of a reflective, linear phase-type grating (of frequency up to 2,000 lines/mm or 50,800 lines/inch) from an interferometrically generated mold to an actual prototype.[3] The technique has rapidly grown in popularity since its introduction in 1980 because it offers very high sensitivity, excellent contrast and good spatial resolution.[4]

In conventional moire interferometry, a reflective phase-type sinusoidal grating is generated interferometrically and transferred to a specimen. The sinusoidal grating diffracts practically no light into the harmonic orders greater than 1, and only the -1 and +1 diffraction orders can be combined to create an interferometric fringe pattern. In this case, the sensitivity is fixed at half the pitch of the specimen grating. This fixed sensitivity requires that the investigator have some prior knowledge of the magnitude of the displacement to be studied, and places restrictions on the examination of regions in which high strain gradients occur.

This paper presents a method for achieving variable sensitivity moire interferometry. The approach relies on a new, extremely precise process called optical microlithography to produce a silicon wafer mold for transferring a grating to a specimen surface. A square wave profile is used to demonstrate the feasibility of the method. The surface characterization of the etched wafer is discussed and equations are presented to describe the interference and diffraction characteristics of the reflective square wave grating. Experiments are then performed in which surface displacements are measured using different diffraction order pairs.

Analysis

In variable sensitivity moire interferometry a silicon wafer mold is produced so that a grating can be transferred to a specimen. The specimen is symmetrically illuminated with coherent light at angles α_m such that the +m and -m diffraction orders propagate collinearly along a path normal to the grating surface. The illuminating beams produce a virtual grating on the surface having a spatial frequency, f_v, given by

$$f_v = (2\sin\alpha_m)/\lambda \qquad [1]$$

where λ is the wavelength of the illuminating source. When the specimen is loaded, the diffracted wavefronts interfere to produce a pattern which can be described in terms of the conventional moire equation

$$U = Np \qquad [2]$$

where N is the fringe order number and p is the pitch of the reference grating ($1/f_v$). In the case of variable sensitivity moire interferometry, the spatial frequency of the virtual grating is 2m times that of the fundamental frequency, f, of the specimen grating. Therefore, the displacement measured perpendicular to the lines in the reference grating is given by

$$U = N/f_v = N/2mf. \qquad [3]$$

Equations 1-3 show that in-plane displacement is measured

---

[1] Dr. Johnson-Cole is a senior engineer at Teledyne Brown Engineering, Huntsville, Alabama; Mr. Bennewitz is a member of the technical staff at AT&T Bell Laboratories in Allentown, Pennsylvania; and, Dr. Gilbert is professor of mechanical engineering at the University of Alabama in Huntsville, Huntsville, Alabama.

with a sensitivity that depends on the pitch of the specimen grating and the diffraction order pair being used. To achieve variable sensitivity, a high quality grating is required which has a symmetric profile sufficient to diffract a usable amount of light into a variety of orders. This paper demonstrates that the method of optical microlithography can be used to create such a grating.

Optical Microlithography

In the past, most gratings were mechanically ruled and, therefore, could not be produced with a pitch comparable to that of an interferometrically generated grating. However, improved step and repeat systems (wafer steppers) are now meeting the requirements for submicron design rules in the electronics industry. This progress has been driven by many factors including improvements in lens design and fabrication, refinements in optical resists, and the ability to retrofit innovations into existing machines. Current projections indicate that optical microlithography will eventually be used to produce IC devices with less than 0.5 micron design rules.[5-8]

AT&T Bell Laboratories recently developed a deep ultraviolet step and repeat system capable of achieving 0.5 μm resolution within a 14.5 mm field under routine use, and even higher resolution (0.35 μm) under more limited conditions.[9] The major optical components of the stepper are shown in Figure 1.

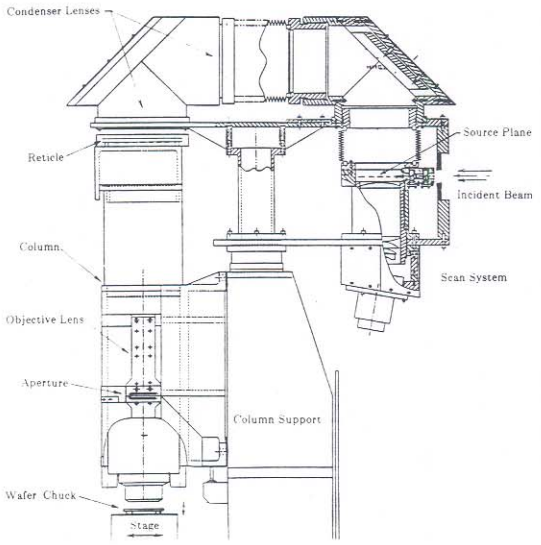

Figure 1. Optical microlithography wafer stepper and projection optics.

Pulsed laser light, from a KrF excimer laser at 248.4 nm, enters the stepper through the diffusing element which serves to scatter the beam spatially, thereby improving the uniformity of the illumination. The light then enters the scan system which is comprised of a scanning mirror and a lens. The mirror deflects the pulses into the lens at different angles; the lens, in turn, focuses the pulses at different points in the source plane. Beyond the source plane, the light diverges to fill the condenser and is then focused into the projection lens. As a result, the condenser forms an image of the source plane at the entrance pupil of the projection lens. The effect of scanning many pulses is to create an extended source of light which is imaged at the entrance pupil. Spatial coherence can be set by controlling the extent of the scan.

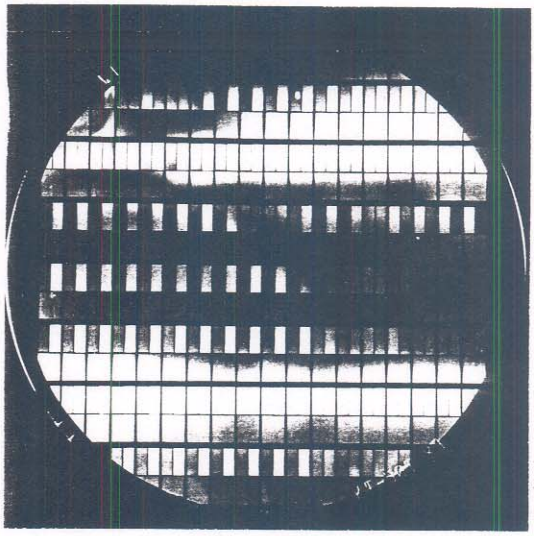

Figure 2. Photograph of the silicon test wafer.

The silicon wafer shown in Figure 2 was manufactured while initially testing this new system. Each small rectangular area contains a regularly structured grating pattern. The spacing and orientation of these patterns form the basis for evaluating the accuracy of the system. An earlier paper by the present authors and their collaborators[10] suggested that this wafer could be used for moire interferometry but attempts to transfer the grating to the specimen met with limited success. One of the major problems can be observed in Figure 3 which shows the magnified image, taken from a scanning electron microscope, of a portion of the surface profile of the wafer. The height of the grating profile is approximately constant at 1 μm, however,

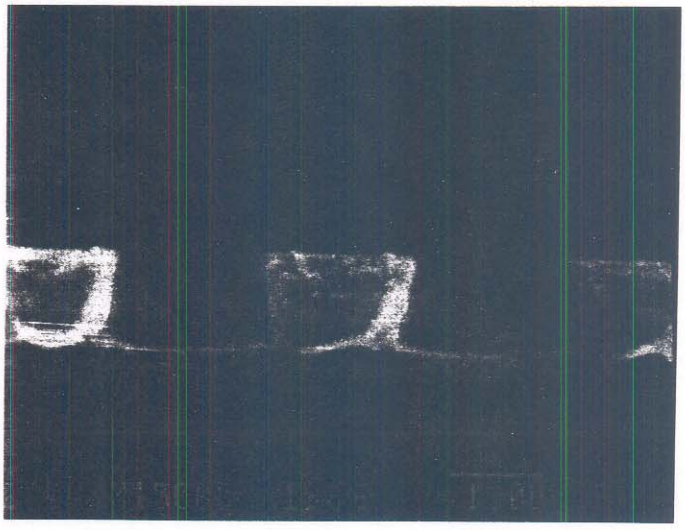

Figure 3. Cross sectional view of a site on the test wafer.

the dove-tail profile of the surface made it difficult to uniformly coat the wafer with a reflective coating and prevented the release of the mold. In addition, the meander patterns on the test pattern were not all of the same pitch. Three different spacings were used to test the layout system capabilities of the stepper system. Therefore, if the wafer was used for moire interferometry, displacements would be measured at different sensitivities in each rectangular area.

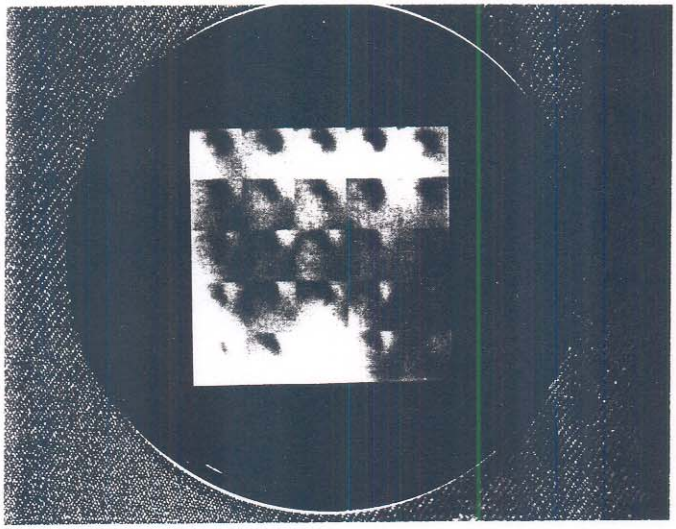

Figure 4. Photograph of a silicon wafer with a crossed, square wave grating.

Figure 4 shows a modified silicon wafer manufactured for use in the present study. This wafer contains a crossed square wave grating pattern that covers a total of 25 cm^2 of the wafer surface. The pattern is comprised of an array of individual squares that each contain an identical crossed square wave grating pattern. The individual square patterned areas are created one at a time and the grating pattern within each square is very closely matched at its boundary with the adjacent squares. The segmentation of the overall grating is due to present limitations on the field size that may be produced with the current system. A comparison is drawn between the original wafer and the modified wafer in the following section.

Surface Characterization

A Nomarski microscope was used to determine the pitch of patterns on the two different silicon wafers shown in Figures 2 and 4. Figure 5 shows microscopic image of the original test wafer taken with a magnification of 69. It clearly shows the three grating test sites. The pitch of the gratings in the upper right, upper left, and bottom areas of the figure are 3.5 μm, 4.0 μm, and 4.5 μm, respectively. Figure 6 shows a photograph (X691) of the modified wafer created for the present investigation where the grating has a two dimensional, crossed square wave profile. The pitch of the grating is 4.0 μm and the crest and trough are both equal to 2.0 μm.

Further characterization of the crossed grating wafer using the scanning electron microscope measured the height of the grating at 0.5 μm, and verified that the profile was extremely close to the intended square wave shape. Even though the square wave grating has a frequency of 250 lines/mm, which is significantly lower than the frequency of the interferometric gratings used in conventional moire interferometry (typically 1200 to 2000 lines/mm), the profile diffracts a number of harmonics which allow displacement to be measured over an extended range.

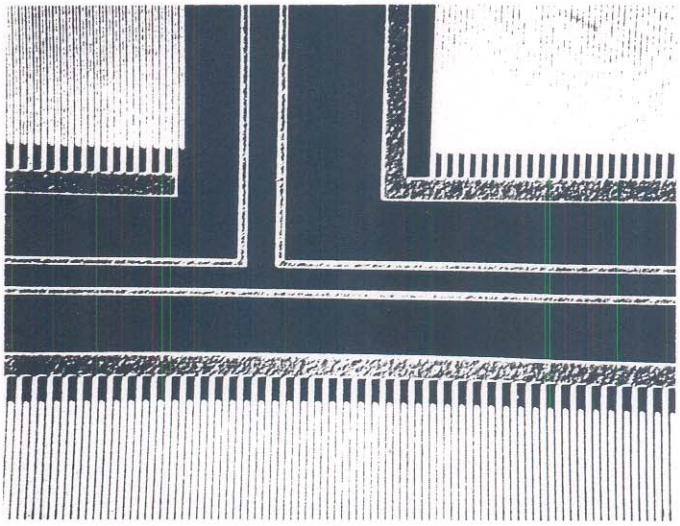

Figure 5. Nomarski microscope image of the silicon test wafer (X69).

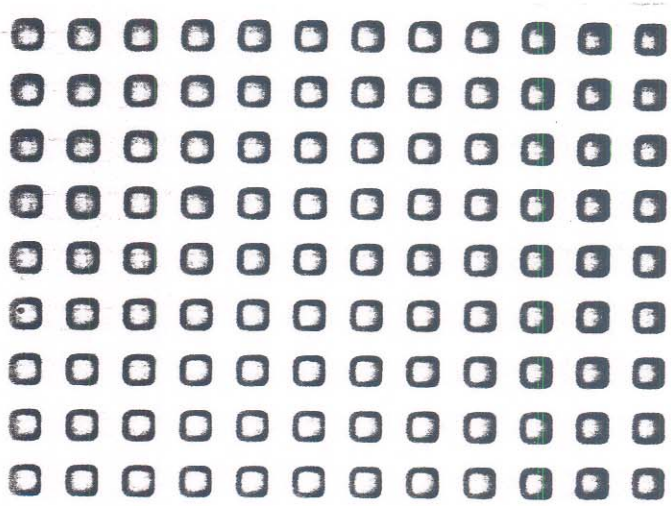

Figure 6. Microscopic image of the silicon wafer with a crossed, square wave grating (X691).

Equations 1 and 3 predict that as many as seven diffraction order pairs may be used for displacement analysis when this square wave grating is illuminated with a wavelength of 514.5 nm. Table 1 lists the seven diffraction order pairs along with the required angle of illumination and resulting sensitivity associated with each possible combination. Provided that light is efficiently diffracted into the appropriate orders, the potential sensitivity range for this grating spans from 2.0 μm/fringe

Table 1. Range of Sensitivity

Angle of Illumination, α_i	Diffraction Order Pair, m	Sensitivity of Measurement, p_s
7.4°	1	2 μm/fringe
14.9°	2	1 μm/fringe
22.7°	3	0.666 μm/fringe
31.0°	4	0.500 μm/fringe
40.0°	5	0.400 μm/fringe
50.0°	6	0.333 μm/fringe
64.2°	7	0.285 μm/fringe

(corresponding to a virtual grating of 500 lines/mm) up to 0.285 μm/fringe (corresponding to a virtual grating of 3,500 lines/mm). The lower sensitivity limit on this range is directly related to the frequency of the specimen grating while the upper end on sensitivity is theoretically never greater than 0.25 μm/fringe.[11] From a practical standpoint, however, the upper sensitivity limit in variable sensitivity moire interferometry is really a function of the grating profile and its associated diffraction efficiency and interference characteristics. These factors are discussed below.

Interference and Diffraction Characteristics

The optical interference and diffraction characteristics of a grating are directly linked to the grating profile through electromagnetic grating theory. Figure 7 shows the result of illuminating a portion of the original test wafer with an unexpanded laser beam. Since the surface profile of the test pattern is a square wave, multiple diffraction orders are produced. The diffraction spectrum is comprised of the fundamental harmonic corresponding to the frequency of the grating plus higher order harmonics. The angular separation of the diffracted orders is a function of the pitch of the grating and the wavelength of the illuminating light.

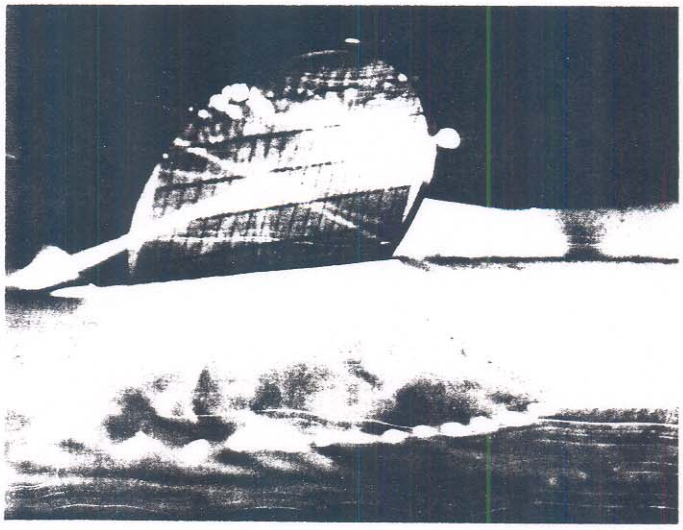

Figure 7. Illumination of the test wafer with a 514.5 nm wavelength source.

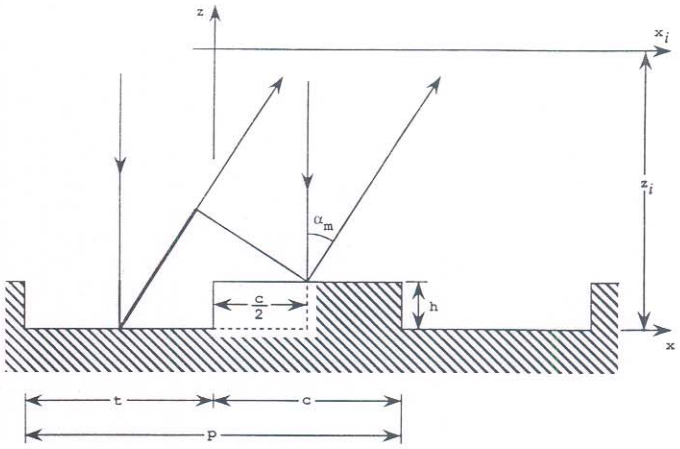

Figure 8. Diffraction from a reflective square wave profile.

Figure 8 shows a coherent beam of light with wavelength λ, illuminating a one dimensional reflection phase type grating. All beam propagation directions are assumed to be in the (x,z) plane. The law governing the grating diffraction is

$$\sin(\alpha_m) = \sin(\alpha_i) + (m\lambda/p) \qquad [4]$$

where p is the pitch of the grating, m is the diffraction order, and α_m and α_i are the diffraction angle and incident angle with respect to the z axis. In the figure, it is assumed that the grating is illuminated by a collimated coherent light source in a direction normal to the grating surface (α_i=0). Considering a ray trace through one period,[12] the reflectance function can be written as

$$r(x) = [\text{rect}\frac{(x-(c/2))}{c} + \text{rect}\frac{(x+(t/2))}{t}\ \exp(jk(2h))] * \text{comb}(x/p) \qquad [5]$$

where c is the crest, t is the trough, h is the height, and p is the pitch of the grating. The rect functions indicate the profile shape, the complex term accounts for the phase delay of the trough, and the comb function is a grating array factor.

The field strength of the Fraunhofer diffraction pattern for r(x) is found using

$$U(x_i) = (1/j\lambda z_i)\exp[jk(z_i + (x_i^2/2z_i)]\ R(f) \qquad [6]$$

where R(f) is the Fourier transform of the reflectance function. R(f) can be written

$$R(f) = \{c\ \text{sinc}(cf)\exp(-j\pi fc) + t\ \text{sinc}(tf)\exp[j(2kh + \pi ft)]\}p\ \text{comb}(pf) \qquad [7]$$

where the sinc function is the transform of the rect function and f is the spatial frequency. The intensity field distribution is found by multiplying U(f) by its complex conjugate. That is

$$I(f) = U(f)\ U(f)^*. \qquad [8]$$

Using Equations 6 and 7, Equation 8 is written as

$$I(f) = (-1/(\lambda z_i)^2)[c^2\text{sinc}^2(cf) + t^2\text{sinc}^2(tf) + ct\ \text{sinc}(cf)\text{sinc}(tf)\{2\cos(\pi fc + 2kh + \pi ft)\}]p^2\text{comb}(pf). \quad [9]$$

For a square wave grating with equal crest and trough dimensions, Equation 9 reduces to

$$I(f) = -(cp/\lambda z_i)^2\text{sinc}^2(cf)[2 + 2\cos(2\pi fc + 2kh)]\text{comb}(pf) \quad [10]$$

where t is set equal to c.

This relatively simple one-dimensional analysis can be applied to the crossed grating prepared for this investigation which has equal trough and crest dimensions of 2 μm, a pitch, p, of 4 μm, and a height, h, of 0.5 μm. When illuminated with a coherent source, a diffraction field, described by Equation 10, is located z_i from the grating. Using a wavelength of 514.5 nm, the relative intensity distribution can be plotted using a commercially available software package and is shown in Figure 9. As indicated by the comb function in Equation 10,

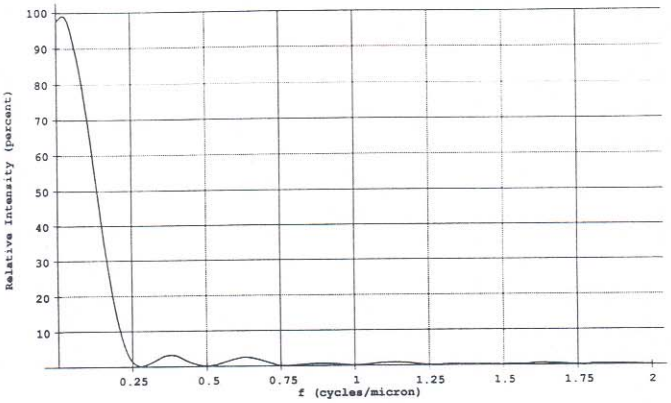

Figure 9. Diffraction field intensity distribution from a reflective square wave grating with c=2.0 μm, t=2.0 μm, and h=0.5 μm.

the first diffraction order, corresponding to the fundamental grating frequency, is located at 0.25 cycles/μm; higher order harmonics are located at integer multiples of the fundamental frequency. The diffraction efficiency for each diffraction order can also be obtained from Figure 9 and is listed in Table 2.

Table 2. Diffraction Efficiency of Existing Grating

Diffraction Order	Harmonic Frequency	Diffraction Efficiency
0	0 cycles/μm	97.11 %
1	0.25 cycles/μm	1.25 %
2	0.50 cycles/μm	0.00 %
3	0.75 cycles/μm	0.14 %
4	1.00 cycles/μm	0.00 %
5	1.25 cycles/μm	0.05 %
6	1.50 cycles/μm	0.00 %
7	1.75 cycles/μm	0.02 %

The figure also illustrates that over 97 percent of the light incident on the grating is directly reflected into the zeroth order; consequently, only 3 percent of the incident light is diffracted by the remaining harmonics. In addition, the relative intensity of the even diffraction orders is diminished because the even harmonics coincide with the zeros of the sinc(cf) function. This occurs because the grating profile used in this study has a crest equal to half the pitch. In addition, the square wave profile produces relatively low diffraction efficiency for odd orders above 3.

The intensity of the odd diffraction orders would be greater if the odd harmonics of the fundamental frequency coincided with maximas of the interference (cosine) term in Equation 10. This could be accomplished in future research by changing the height of the grating profile, h.

Another variation of the existing square wave profile could be used to increase the relative diffraction efficiency in both the even and odd harmonic orders. By altering the grating dimensions of the crest and trough, the diffraction envelope can be widened to allow the working orders to lie within the main lobe. By decreasing the crest, c, of the grating profile, the main lobe of the sinc(cf) term in Equation 9 is widened. For example, by choosing a crest of 0.5 μm and a trough, t, of 3.5 μm the main lobe of sinc(cf) extends its first zero out to a frequency of 2 cycles/μm. This prevents any of the first seven diffraction orders from coinciding with the zeros of the sinc(cf) term. In addition, h, can be chosen so that the peaks of the interference (cosine) term are aligned with the harmonic frequencies. Figure 10 shows the diffraction field, relative intensity distribution that results for such a grating profile when illuminated with a wavelength of 514.5 nm. Table 3 lists the corresponding diffraction efficiencies for each of the diffraction orders. Since the pitch of this grating profile has not been changed from the equal crest and trough grating discussed in both cases above, the harmonic frequencies of the diffraction orders remain unchanged. Moreover, the even orders diffract an appreciable percentage of the incident light, and the efficiencies of the first seven diffraction orders are relatively good.

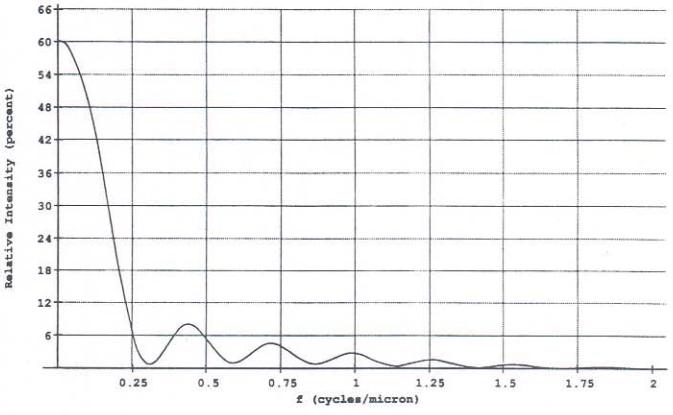

Figure 10. Diffraction field intensity distribution from a reflective square wave grating with c=0.5 μm, t=3.5 μm, and h=(g+1)λ/4.

Table 3. Diffraction Efficiency of Grating with Crest of 0.5 μm, Trough of 3.5 μm, and Optimized Height

Diffraction Order	Harmonic Frequency	Diffraction Efficiency
0	0 cycles/μm	59.12 %
1	0.25 cycles/μm	6.24 %
2	0.50 cycles/μm	5.32 %
3	0.75 cycles/μm	4.04 %
4	1.00 cycles/μm	2.66 %
5	1.25 cycles/μm	1.45 %
6	1.50 cycles/μm	0.59 %
7	1.75 cycles/μm	0.13 %

In summary, the crossed grating wafer prepared for this investigation fails to exhibit optimal diffraction efficiency in the higher diffraction orders; nonetheless, this grating is sufficient to demonstrate the feasibility of variable sensitivity moire interferometry as described in the following paragraphs.

Variable Sensitivity Experiments and Results

Two experiments were performed to demonstrate the variable sensitivity method. The first experiment combines the third order diffraction pair and uses the carrier fringe/double exposure technique to study the fringe field that results from a known loading state. The second experiment demonstrates that the third and fifth order diffraction pairs can be used simultaneously to measure displacement at different sensitivities. Both of these experiments require that a grating be transferred from the silicon wafer to the test surface. The transfer process is discussed next, after which the experiments are detailed.

A very weak solution of Kodak Photoflow in deionized water was spun onto several bare crossed grating wafers before coating them with aluminum. The wafers were allowed to spin until fairly dry. Next they were placed in a desiccative environment and, when thoroughly dry, overcoated with aluminum. For this process, the wafers were placed in a planetary vacuum deposition chamber and overcoated with a layer of aluminum, approximately 3000 angstroms thick. They were slowly rotated during the deposition process to insure even coating of the walls of the grating.

A thin coat of epoxy was initially applied to the specimen and the epoxied surface was placed face down on the aluminized wafer. The edges of the specimen were carefully aligned with the cross grating to provide a means for measuring orthogonal displacement components. After the epoxy cured, the specimen was pried loose taking great care not to break the wafer. Excess epoxy was removed.

Figure 11 shows the experimental set-up used to record interferometric moire patterns with variable sensitivity from a grating deposited on the surface of the notched beam shown in

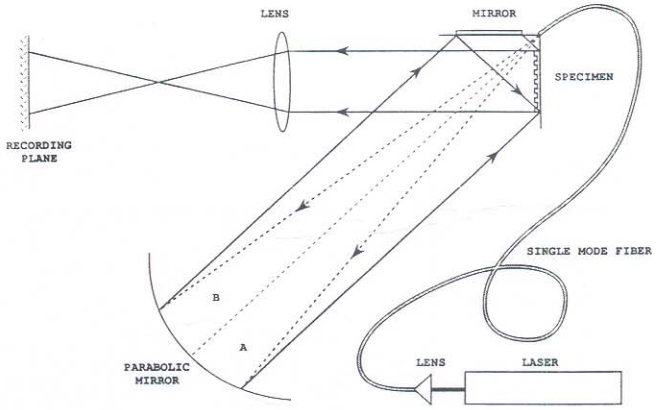

Figure 11. Experimental set-up for moire interferometry.

Figure 12. An unexpanded argon ion laser beam of 514.5 nm wavelength was launched into a single mode step index fiber using a 5X microscope objective. The exit end of the fiber was placed at the focal point of an on-axis parabolic mirror (2 m focal length, 0.41 m diameter), thereby, producing a collimated beam with Gaussian intensity distribution. The parabolic mirror reflected the collimated light back to the specimen holder assembly where a flat mirror was positioned at 90 degrees to the specimen. Rotation of the entire assembly about a vertical axis controlled the angle of illumination. The notched beam was placed in three point bending and the stage was oriented to symmetrically illuminate the specimen at an angle of 22.7 degrees with respect to its normal. This illumination angle corresponds to the third diffraction order pair; Table 1 shows that displacement is measured at a sensitivity of 0.666μm/fringe. As illustrated in Figure 11, the -3 diffraction order from beam A coincides with the +3 diffraction order from beam B. Both wavefronts are diffracted along the normal to the specimen surface and pass through a 38.1 mm diameter, 375 mm focal length imaging lens.

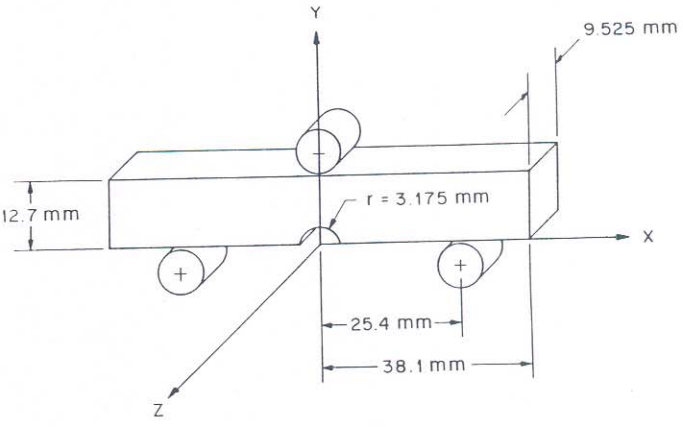

Figure 12. Dimensions of circularly notched beam specimen.

Since the longitudinal axis of the notched beam was oriented parallel to the lines in the interference zone of the two illuminating plane waves, the displacement component measured was perpendicular to its longitudinal axis. A carrier pattern, or linear phase shift between the two diffracted wavefronts, was introduced by rotating the specimen in the plane of the specimen grating. The initial pattern, corresponding to the pre-load condition, was photographed in the image plane and is shown in Figure 13a. Figure 13b shows a photograph of the modulated carrier pattern after the two rollers supporting the beam were displaced 0.0038 mm (.00015") to the left. A double exposure of the initial carrier pattern superimposed with the modulated carrier pattern is shown in Figure 14. The moire fringe pattern represents the full-field in-plane displacement field along the transverse direction of the specimen. Since this component is measured along the y axis, it referred to as the V displacement field. Numbers may be assigned to the moire fringes starting with zero at the center support; consequently, the fringe order number at the outer support is 5.5. Equation 1 establishes the pitch of the virtual grating, p_v, at 1/1500 mm. Using Equation 3, the transverse displacement component, V, at the outer beam support is calculated at 0.0037 mm. The interferometrically measured displacement agreed closely with the imposed value of 0.0038 mm.

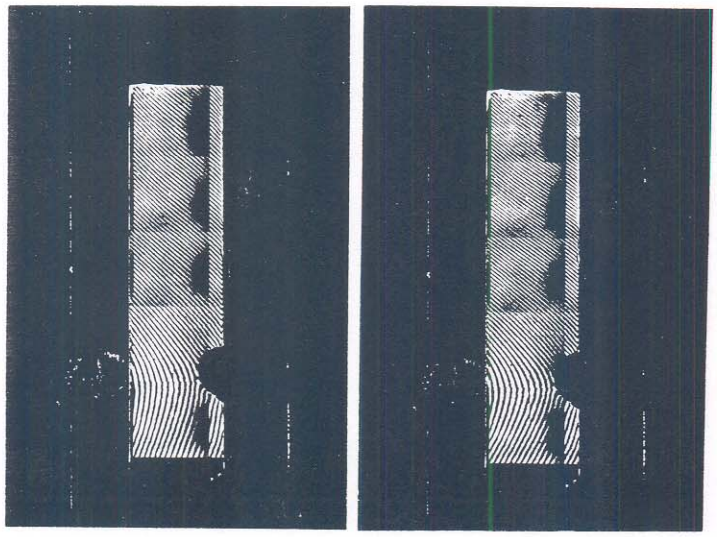

(a) (b)

Figure 13. The V displacement field; (a) initial carrier pattern, (b) modulated carrier pattern.

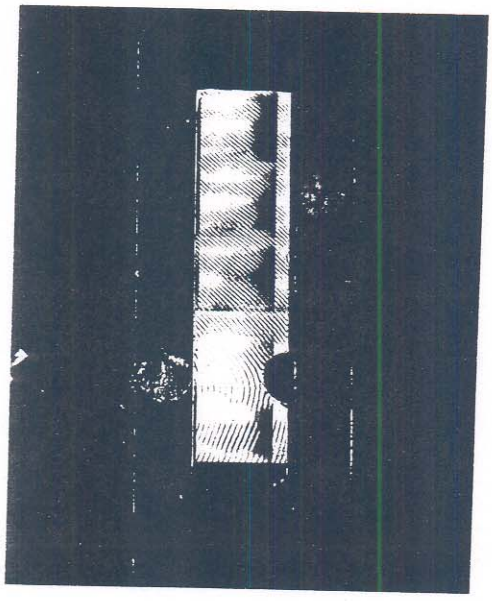

Figure 14. Double exposure of the initial and modulated carrier patterns for the V displacement field.

The experiment described above was repeated to determine the U displacement field along the longitudinal axis of the notched beam. The beam was oriented with its longitudinal axis perpendicular to the lines in the interference zone of the two illuminating wavefronts and the same procedure described above was applied. Figure 15a shows the initial pattern recorded after a carrier was introduced; Figure 15b shows the modulated pattern after the load was applied. The superposition of these patterns is shown in Figure 16. Moire fringes may be numbered starting with zero at the center support. Equation 3 can be used to obtain the U displacement.

A second experiment was conducted to demonstrate that moire patterns having different sensitivity could be recorded simultaneously. Figure 17 shows an argon ion laser beam expanded by a spatial filter and collimated using a lens. The collimated beam was directed to the specimen holder assembly where it illuminated the specimen and a flat mirror positioned

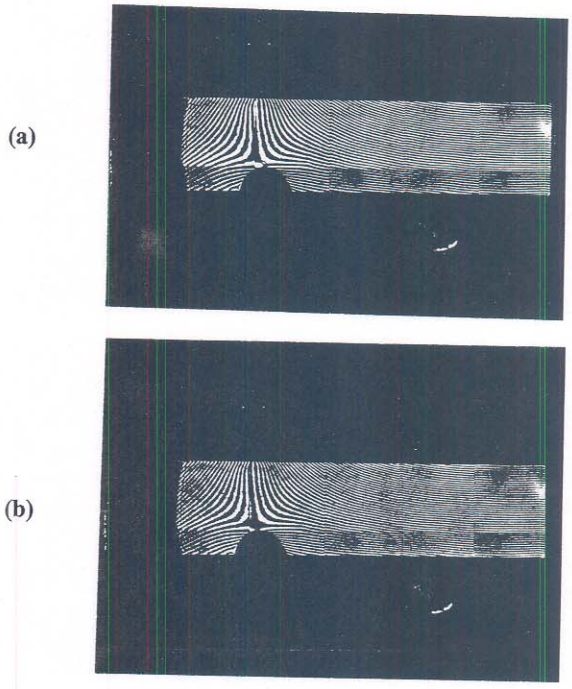

(a)

(b)

Figure 15. The U displacement field; (a) initial carrier pattern, (b) modulated carrier pattern.

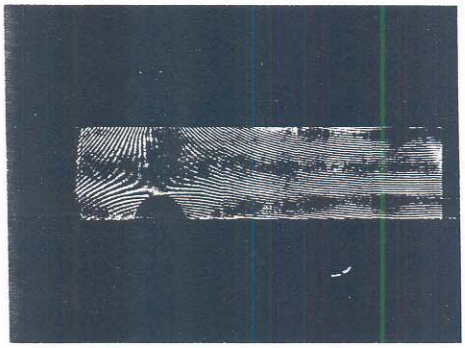

Figure 16. Double exposure of the initial and modulated carrier patterns for the U displacement field.

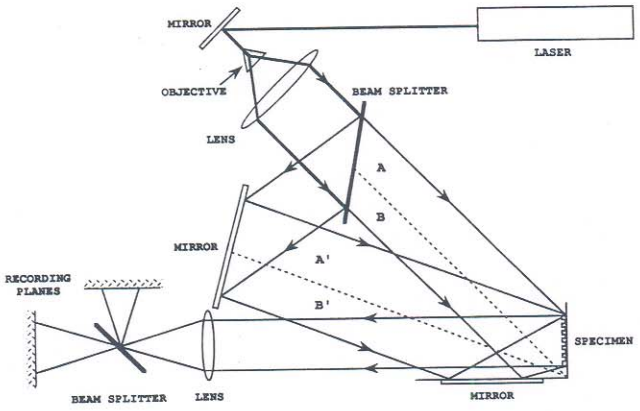

Figure 17. Experimental set-up for simultaneously recording displacement at two different sensitivities.

at 90 degrees to the specimen surface. The specimen holder assembly was rotated about a vertical axis and positioned such that the propagation vector of the illuminating beam made a 40 degree angle with respect to the specimen grating normal. This orientation was chosen to create a virtual grating (formed in space due to the interference of the direct beam, A, and the reflected beam, B) having a spatial frequency ten times that of the specimen grating. A beam splitter was placed in the collimated illuminating beam and the split beam was directed at the specimen holder assembly using an adjustable flat mirror. The propagation direction of the collimated split beam was chosen to interrogate the specimen with a virtual grating having a frequency six times that of the real grating. When appropriately illuminated, the -3 and +3 diffraction orders from beams A' and B', respectively, were collinearly diffracted together with the -5 and +5 diffraction orders from beams A and B. In this case, four wavefronts were simultaneously diffracted from the specimen surface along the grating normal!

The notched specimen was placed in a three point bending and the frame was oriented such that the longitudinal axis of the beam was parallel to the lines in the interference zone of the two illuminating wavefronts. This orientation allowed the displacement component perpendicular to the longitudinal axis of the beam to be measured. The optical system was fine tuned to achieve an initial interference pattern for each of the diffraction order pairs being used. This was accomplished by first blocking illuminating beams A and B to produce an initial pattern with the third order diffraction pair, then by blocking beams A' and B' and unblocking beams A and B to yield an initial interference pattern with the fifth order diffraction pair. A vertical carrier pattern was generated by rotating the loading frame assembly about a vertical axis.

The double exposure method was used to study and compare the response of the third order pair and fifth order pair to an identical loading condition. A beam splitter was placed behind a single imaging lens, as shown in Figure 17, to make this comparison possible. A Polaroid camera back was positioned in each of the two image planes of the recording system. Beams A and B were blocked and an initial carrier pattern, produced by the third order diffraction pair, was photographed in recording plane 1. The film positioned in recording plane 1 remained undisturbed. Then beams A and B were unblocked and beams A' and B' were blocked. The film in recording plane 2 was then exposed to an initial carrier pattern produced by the fifth order pair. Next, the model was loaded by displacing the two rollers supporting the notched beam to the left. The film in recording plane 2 was exposed to the fifth order diffraction pair for a second time, but this time it was exposed to a modulated carrier pattern corresponding to the load induced condition of the model. Finally, beams A' and B' were unblocked and beams A and B were blocked and the previously exposed film in recording plane 1 was exposed to the modulated carrier pattern produced by the third order diffraction pair.

Figure 18 shows a double-exposure recording of the initial and modulated carrier patterns produced by the third diffraction order pair. Similarly, Figure 19 shows the double-exposure moire interferometry recording that was produced using the fifth order pair. The patterns are transposed due to the

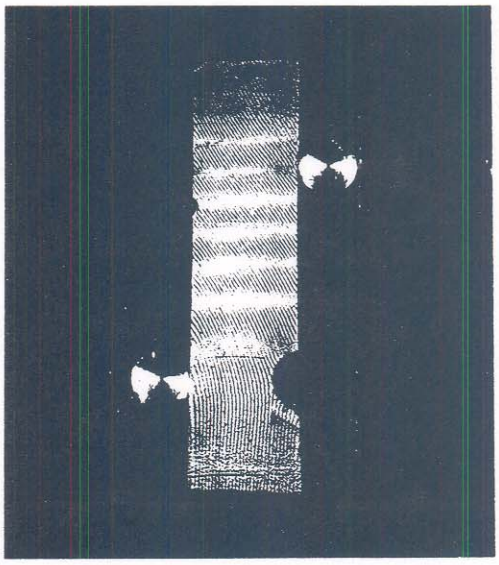

Figure 18. Interferometric moire pattern with sensitivity of 0.666 microns/fringe.

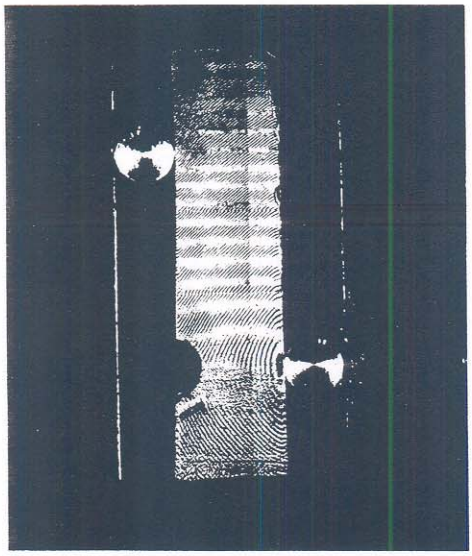

Figure 19. Interferometric moire pattern with sensitivity of 0.400 microns/fringe.

reflection at the splitter. Moire fringe order numbers were assigned in both figures starting with zero at the center support above the notch.

A comparison of Figures 18 and 19 verifies Equation 3, and illustrates that the sensitivity is governed in part by the diffraction orders used. From Table 1, moire fringes recorded using the third diffraction order pair have a sensitivity of 0.666 μm/fringe while the sensitivity of measurement using the fifth order diffraction pair is greater and equal to 0.400 μm/fringe. Equation 3 dictates that points contained within the fringe distribution shown in Figure 19 should have a fringe order number that is 1.666 times the fringe order number of the corresponding point in Figure 18. This can be verified quantitatively by considering the fringe order numbers at the outer roller support. In Figure 18 the fringe order at this location is approximately 5.5 while the fringe order number at the corresponding point in Figure 19 is approximately equal to 9.0, making the ratio roughly 1.6.

Discussion

This paper has clearly demonstrated that optical microlithography offers many distinct advantages over the more conventional interferometric method for producing diffraction gratings suitable for moire interferometric analysis. Future research could capitalize on analytical arguments contained herein to design and produce grating profiles with multiple diffraction orders having high diffraction efficiencies. The profile could be shaped to facilitate coating of the wafer and transfer of the grating to the specimen; for example, by making the profile triangular. In addition to creating profile shapes impossible to achieve interferometrically, optical microlithography could also be used to fabricate gratings with geometries specifically tailored to a particular application. For example, a set of equally spaced concentric circles could be produced to study radial displacements in the neighborhood of a crack tip. New replication techniques could be developed so that several submasters can be produced from a single silicon wafer. This would facilitate technology transfer and make the overall approach to moire interferometry more economical.

Conventional moire interferometry is currently limited to the analysis of flat surfaces. However, the technique could be applied to curved surfaces by coating a specimen with photoresist and then by exposing the photoresist in the interference zone of two plane wavefronts. Once developed, the specimen would be realigned so that light from the two beams was appropriately diffracted. Unfortunately, this interferometric approach to grating production would result in fringe patterns which would have to be analyzed on a pointwise basis, since sensitivity would vary according to the surface geometry. However, this dependency on geometry could be taken into consideration by producing a customized grating on a silicon wafer using a computer controlled wave stepper. The grating could be transferred to a flexible silicon rubber submaster and then to the specimen. The specimen grating would be coated and, when illuminated, would diffract light sufficient to measure displacement components with a fixed sensitivity over the full field.

Conclusion

Conventionally, the gratings used in moire interferometry are created interferometrically and diffract all usable light into the -1 and +1 diffraction orders, thereby fixing the sensitivity of measurement at half the pitch of the specimen grating. An alternative approach to grating production was developed in this paper where it was shown that optical microlithography could be used to manufacture specialized gratings of nearly any shape and size. The technique was used to produce a square wave grating with a profile having equal crests and troughs. The grating diffracted light into multiple orders and tests were conducted to show that different diffraction orders could be used to vary displacement sensitivity once the grating was transferred to the surface of a test specimen.

The Fraunhofer diffraction approximation was applied to describe the diffraction and interference characteristics of a reflective square wave profile with general dimensions. The square wave grating manufactured for the study was characterized by this approach, only to discover that the diffraction efficiencies of all orders greater than one were extremely poor. This finding was somewhat encouraging, however, since the feasibility for varying sensitivity was successfully demonstrated under much less than desirable conditions. Alternative profiles were discussed and suggestions made for future research.

Acknowledgements

The authors wish to express their thanks to Mr. Curtis Barr of MSFC/NASA for helping to coat the wafers, Dr. Jean Bennett of China Lake Naval Weapons Research Laboratory for helping to characterize the profiles, and Dr. Victor Pol of AT&T Bell Laboratories in Murray Hill, New Jersey for helping with wafer production.

References

1. Dally, J.W., Riley, W.F., Experimental Stress Analysis, 1st Ed., McGraw-Hill, New York, 1965.
2. Post, D., "Moire Interferometry at VPI & SU," Experimental Mechanics, 23(2): 203-210 (1983).
3. Post, D., "Moire Interferometry," Handbook on Experimental Mechanics, Chap. 7, ed. A.L. Kobayashi, Prentice Hall, Englewood Cliffs, NJ, 1987, pp. 314-384.
4. Post, D., "Moire Interferometry: Advances and Applications," Proc. of the 1990 Int. Conf. on Hologram Interferometry & Speckle Metrology, Baltimore, Maryland, November 1990, pp. 1-13.
5. Pol, V., Bennewitz, J.H., Escher, G.C., Feldman, M., Firtion, V.A., Jewell, T.E., Wilcomb, B.E., Clemens, J.T., "Excimer Laser-based Lithography: A Deep Ultraviolet Wafer Stepper," Proc. of the SPIE Conference on Optical Microlithography V, Vol. 633, March 1986, pp. 6-16.
6. Miller, V., Stover, H.L., "Submicron Optical Lithography," Solid State Technology, 29(1): 127 (1985).
7. Shiotake, N., Yoshida, S., "Recent Advances of Optical Step-and-repeat Systems," Proc. of SPIE Conference on Electron-Beam, X-Ray, and Ion-Beam Techniques for Submicrometer Lithographies IV, Vol. 537, March 1985, pp. 168-174.
8. Nakase, M., "The Potential of Optical Lithography," Proc. of SPIE Conference on Electron-Beam, X-Ray, and Ion-Beam Techniques for Submicrometer Lithographies IV, Vol. 537, March 1985, pp. 160-167.
9. Bennewitz, J.H., Escher, G.C., Feldman, M., Firtion, V.A., Jewell, T.E., Pol, V., Wilcomb, B.E., Clemens, J.T., "Excimer Laser-based Lithography for 0.5 Micron Device Technology," Proc. of the IEEE/IEDM Conference, Los Angeles, CA, December 1986, pp. 312-315.
10. Johnson, H.S., Gilbert, J.A., Dudderar, T.D., Bennewitz, J.H., Matthys, D.R., "New Methods for Recording and Processing High Frequency Moire Patterns," Proc. 1987 SEM Spring Conference on Experimental Mechanics, Houston, TX, June 1987, pp. 62-70.
11. Weissman, E.M., Post, D., "Moire Interferometry Near the Theoretical Limit," Applied Optics, 21(9): 2558-2562 (1982).
12. Lizuka, K., Engineering Optics, 2nd Ed., Springer-Verlag, 1987, pp. 77-102.